Aerospace Science and Technology 155 (2024) 109597

Contents lists available at ScienceDirect

Aerospace Science and Technology

journal homepage: www.elsevier.com/locate/aescte

Relative position estimation using modulated magnetic field for close proximity formation flight

Takuma Shibata [a,*], Halil Ersin Söken [b], Shin-ichiro Sakai [c]

[a] Department of Mechanical, Aerospace and Materials Engineering, Muroran Institute of Technology, 27-1, Mizumoto-cho, 050-8585, Muroran, Japan
[b] Aerospace Engineering Department, Middle East Technical University, Cankaya, Ankara, 06800, Turkey
[c] Japan Aerospace Exploration Agency/Institute of Space and Astronautical Science, 3-1-1, Yoshinodai, Chuo-ku, Sagamihara, 252-5210, Japan

ARTICLE INFO

Communicated by Jayaram Sanjay

Keywords:
Relative position estimation
Spacecraft formation flight
Close proximity operation
AC magnetic field

ABSTRACT

This paper presents a method to estimate relative position vectors between spacecraft equipped with magnetic coils and magnetic field sensors for close proximity operation. Filters can segregate a magnetic field with a particular frequency if spacecraft drive their coils with this specific frequency. The proposed method utilizes the amplitude of the magnetic field with a particular frequency to estimate relative position vectors. The method consists of an initial position estimator and a sequential position estimator, which is an unscented Kalman filter. The initial position estimator provides a coarse estimate for the relative position vectors using the segregated magnetic field. Relation between the magnetic field and relative position vector is derived analytically in this article for the initial position estimator. The unscented Kalman filter refines the estimation accuracy by initializing the filter with the estimate by the initial position estimator. It is shown that a spacecraft can conduct relative position vector estimation using the magnetic field of a target spacecraft, provided that a few conditions clarified in the article are satisfied. Finally, the proposed estimators are evaluated numerically via simulations.

1. Introduction

In recent years, large satellites have been used for astronomy and Earth observation, and they have been producing noteworthy results. The larger the optical equipment, the higher target resolution images can be acquired. However, cost and development time for large spacecraft is a primary concern. Moreover, if the spacecraft fails, the whole mission fails. As a solution to this problem, Formation Flight (FF), specifically with small satellites, has been studied as a breakthrough in space technologies. FF technologies have been already demonstrated by GRACE [1,2], GRAIL [3], Tandem-X and TerraSAR-X [4,5], and PRISMA [6,7] missions in space. In many of these FF missions, thrusters control the relative orbit between satellites. As to the other methods, Electromagnetic Formation Flight (EMFF) [8–13] has been studied. Compared with the FF using thrusters, whose mission term is limited by fuel, EMFF have the potential to be used for a longer duration.

Accurate relative position estimation is essential to control the relative orbit, especially for close proximity formation flight. GPS is one of the options to determine the relative orbit [14,15]. In the PRISMA mission, carrier-phase differential GPS (CDGPS) was employed and achieved a relative position error of a few centimeters [16]. For CDGPS, however, all satellites should receive signals from the same GNSS satellites. In addition to the GPS technique, vision-based methods are powerful in determining the relative position and attitude [17,18]. However, the target satellite should be in the image sensor's field of view (FoV). Also the illumination conditions must be favorable and stable, which is difficult to have in space. Moreover, laser range finders are also a considerable option to measure the relative position with high accuracy [19]. However, to get measurements, the spacecraft should hit the laser beams to the target spacecraft in formation, which imposes strict constraints on relative rotational and translational motions similar to the vision-based methods.

As a specialized method for the EMFF, the relative position can be estimated with millimeter accuracy by measuring the frequency-multiplexed magnetic fields [20]. The approach uses induced voltage by the other coils driven with multiple frequencies for relative position and attitude estimation. This method applies to a telescope comprising mirror segment satellites whose relative positions are adjusted using the EMFF technique. This approach was evaluated with the condition that all satellites have three magnetic coils driven with different frequencies. Although an experiment is conducted to evaluate this method, it is tested in a region where the induced voltages are accurately known

* Corresponding author.
E-mail addresses: takuma.shibata@muroran-it.ac.jp (T. Shibata), esoken@metu.edu.tr (H.E. Söken), sakai@isas.jaxa.jp (S. Sakai).

https://doi.org/10.1016/j.ast.2024.109597
Received 28 April 2024; Received in revised form 20 July 2024; Accepted 14 September 2024
Available online 23 September 2024

with respect to the relative position and attitude. This approach cannot solve the real-time relative position and attitude estimation problem. Using a look-up table is proposed as the solution. However, it is not suitable for real-time operation as also mentioned by the authors. In addition to the above method, position and attitude estimation using the magnetic field has been studied for local positioning systems in robotics [21,22] and medical fields [23]. In the Ref. [21], a method to estimate relative position and attitude using the magnetic field is proposed. Although this method enables a full 6-degrees-of-freedom pose estimation, it only works for small angles. In addition, Ref. [22] presents a method to estimate the location of a robot by measuring the magnetic field. This study analytically derives the relation between the absolute position and the magnetic field. By measuring the magnetic field by multiple magnetic field sensors (MFSs) at known locations, localization of the robot is achieved in the same way as the GPS functions. In another study, a method to position MFS in the patient's body is studied for surgery, [23]. By using two magnetic coils at a known location, the attitude and location of MFS in the patient's body can be estimated to increase the success rate of the surgery. These above methods are effective, but the locations of magnetic coils or MFSs should be accurately known. Therefore, multiple spacecraft should cooperate to estimate a target spacecraft position when these methods are applied.

This paper investigates a method to estimate the position vector of an orbiting target spacecraft for proximity formation flight by using two MFSs. In comparison with [20], the proposed method can provide a solution of relative position using the measured magnetic field. A target can be found even if the position is completely unknown initially. In addition, this method works when the relative position between spacecraft dynamically changes and does not require a fixed formation. Last, the proposed method is easy to apply on a spacecraft system using the MFSs, which are technically not complex equipment. The MFSs measure the Alternating Current (AC) magnetic field modulated with specific single-frequencies for all spacecraft in the formation to estimate the relative position vector. The modulation frequencies are unique in the formation, and this uniqueness serves for identifying each spacecraft. When the other spacecraft is orbiting in close proximity, MFSs on the spacecraft can measure collective sum of all the frequency components for the magnetic field. Our approach to segregating the magnetic field with a target frequency employs the Band-Pass Filter (BPF). Due to sampling frequency of the MFS, available frequencies are limited for the BPF. Therefore, a single-frequency is given to each spacecraft in this study. Using the amplitude of the magnetic field filtered by the BPF, the relative position vector is estimated using the proposed method consisting of two different estimators for initial and sequential position estimations. For the initial position estimator, the relation between the magnetic field and relative position vectors is analytically derived in this paper. The sequential position estimator uses an Unscented Kalman Filter (UKF). The proposed method is evaluated by numerical simulation, and the performance and limitations of the proposed method are discussed. We assume that the proposed method is applied to the EMFF. However, it is compatible with any FF method if the spacecraft has coils and MFSs.

2. Dynamics with AC driven magnetic field

EMFF spacecraft can apply magnetic force to only specific spacecraft in the formation by driving their magnetic coils with specific frequencies. This technique, which is called the grouping method in this paper, has been discussed and studied so far in [24,25]. Thanks to this grouping method, it can be assumed that disturbance force and torque caused by our proposed method do not greatly affect the formation control.

Considering spacecraft $\mathbb{P} \in \{1,2,3,4,...,N\}$ are orbiting nearby, spacecraft q attempts to form a group with spacecraft $\mathbb{S} = \{s | s \in \mathbb{P}, s \neq q\}$. The spacecraft q achieves this by driving the coils to generate the following magnetic moment vector:

$$\begin{aligned} \boldsymbol{M}_q &= \left[M_{xq}, M_{yq}, M_{zq}\right]^T \\ &= \sum_{s \in \mathbb{S}} \boldsymbol{m}_{q \to s} \sin(\omega_s t + \phi_q) \end{aligned} \tag{1}$$

where, $\boldsymbol{m}_{q\to s} = \left[m_x, m_y, m_z\right]^T_{q\to s}$ is amplitude of the magnetic moment vector along each axis, ω_s is the angular frequency assigned to target spacecraft s, ϕ_q is the phase shift, and t is time. Generating the magnetic moment vector mixing components with angular frequencies of spacecraft s, the spacecraft q can apply the magnetic force and torque to the spacecraft s. The magnetic field at spacecraft s is given as

$${}^{\mathcal{Q}}\boldsymbol{B}_q = \frac{\mu_0}{4\pi r_{qs}^3} \left\{ -\boldsymbol{M}_q + \frac{3\left(\boldsymbol{M}_q \cdot \boldsymbol{r}_{qs}\right)}{r_{qs}^2} \boldsymbol{r}_{qs} \right\} \tag{2}$$

where, left superscript $\mathcal{Q}$ stands for the spacecraft q fixed frame system, $\boldsymbol{B}_q$ is magnetic field vector generated by the spacecraft q, $\boldsymbol{r}_{qs}$ is relative position vector from the spacecraft q to spacecraft s, and r_{qs} is the norm of the relative position vector $\boldsymbol{r}_{qs}$, which is $r_{qs} = ||\boldsymbol{r}_{qs}||$. Using the Eq. (1) together with the Eq. (2), the total magnetic force $\bar{\boldsymbol{F}}_{q\to s}$ in one cycle time $\Delta t = t_f - t_0 = 2\pi/\omega_s$ that is applied on the spacecraft s by the spacecraft q can be given as [26]

$${}^{\mathcal{Q}}\bar{\boldsymbol{F}}_{q\to s}\Delta t = \boldsymbol{f}_{q\to s} \int_{t_0}^{t_f} \sin(\omega_s t + \phi_s)\sin(\omega_q t + \phi_q) dt \tag{3}$$

where, $\boldsymbol{f}_{q\to s}$ is the magnitude of the magnetic force vector exerted on spacecraft s by spacecraft q. The total magnetic force is finally expressed as follows:

$${}^{\mathcal{Q}}\bar{\boldsymbol{F}}_{q\to s} = \begin{cases} \dfrac{\boldsymbol{f}_{q\to s}}{2}\cos(\phi_s - \phi_q) & \text{if } \omega_s = \omega_q \\ \boldsymbol{0} & \text{otherwise} \end{cases} \tag{4}$$

Similar to the magnetic force, the total magnetic torque $\boldsymbol{T}_{q\to s}$ on the spacecraft s by the spacecraft q in one cycle time Δt is expressed as

$${}^{\mathcal{Q}}\bar{\boldsymbol{T}}_{q\to s}\Delta t = \boldsymbol{\tau}_{q\to s} \int_{t_0}^{t_f} \sin(\omega_s t + \phi_s)\sin(\omega_q t + \phi_q) dt. \tag{5}$$

The Eq. (5) is finally solved as

$${}^{\mathcal{Q}}\bar{\boldsymbol{T}}_{q\to s} = \begin{cases} \dfrac{\boldsymbol{\tau}_{q\to s}}{2}\cos(\phi_s - \phi_q) & \text{if } \omega_s = \omega_q \\ \boldsymbol{0} & \text{otherwise} \end{cases} \tag{6}$$

The total force and torque in one cycle time are expressed similarly. As seen in Eq. (4) and Eq. (6), the magnetic force and torque between spacecraft q and s exist only if the angular frequency ω_q matches to ω_s. Otherwise, averaging over one complete cycle cancels the force and torque. In addition, the magnetic force and torque decrease by phase shift error between coils driven by the spacecraft q and s. The clocks on formation spacecraft should be synchronized so that phase shift error is minimized and there is no torque and force loss. Our proposed method utilizes the property of the grouping method such that the magnetic force and torque do not affect the formation control by driving their magnetic coils with different frequencies.

3. Segregation of magnetic field with a specific single-frequency

Our proposed method aims to estimate relative position vector between spacecraft in formation by measuring the modulated magnetic field with specific single-frequency. It is assumed that multiple spacecraft are orbiting in close proximity with respect to spacecraft q as shown in Fig. 1. Spacecraft q operates the magnetic coils with the additional sinusoidal components in Eq. (1) as

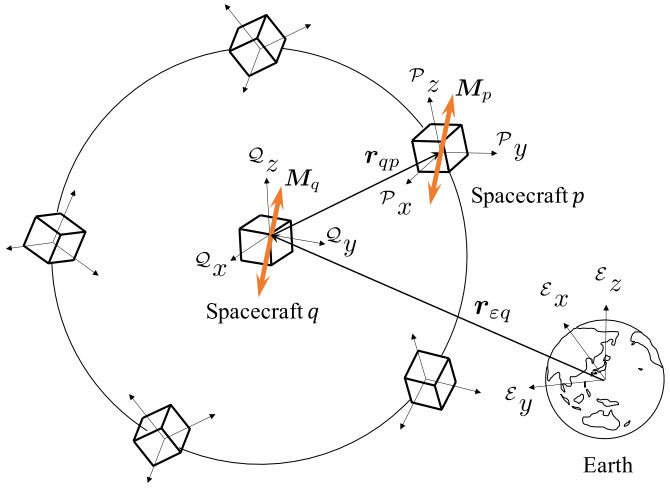

Fig. 1. EMFF spacecraft generating magnetic moment vector with specific frequency for controlling and informing the position to the other spacecraft.

$$
\begin{aligned}
{}^{\mathcal{Q}}\boldsymbol{M}_q &= \sum_{s\in\mathbb{S}} \boldsymbol{m}_{q\to s}\sin(\omega_s t+\phi_q) + \boldsymbol{m}_{\mathrm{E}q}\sin\left(\omega_{\mathrm{E}q}t\right) \\
&= \boldsymbol{M}_{\mathrm{CO}q} + \boldsymbol{M}_{\mathrm{E}q}
\end{aligned} \tag{7}
$$

where, subscripts CO and E specify magnetic moments for control and position estimation respectively. These two moments can be segregated using the BPF in practice. The angular frequency $\omega_{\mathrm{E}q}$ is unique to the formation such that it does not create disturbance force and torque in one complete cycle time. Substituting the Eq. (7) into Eq. (2), magnetic field by the spacecraft q is expressed as a linear combination:

$$
{}^{\mathcal{Q}}\boldsymbol{B}_q = {}^{\mathcal{Q}}\left\{\sum_{s\in\mathbb{S}} \boldsymbol{B}_{\mathrm{CO}q}\left(\boldsymbol{m}_{q\to s},\omega_s\right) + \boldsymbol{B}_{\mathrm{E}q}\left(\boldsymbol{m}_{\mathrm{E}q},\omega_{\mathrm{E}q}\right)\right\}. \tag{8}
$$

Considering spacecraft $p\in\mathbb{P}$ flying nearby the spacecraft q, a MFS on a spacecraft q measures total magnetic field $\boldsymbol{B}_{\mathrm{TOT}}$ as

$$
{}^{\mathcal{Q}}\boldsymbol{B}_{\mathrm{TOT}} = {}^{\mathcal{Q}}\boldsymbol{B}_q + \sum_{p\in\mathbb{P}} \boldsymbol{R}^{\mathcal{Q}/\mathcal{P}}\cdot{}^{\mathcal{P}}\boldsymbol{B}_p + {}^{\mathcal{Q}}\boldsymbol{B}_d \tag{9}
$$

where, $\boldsymbol{R}^{\mathcal{Q}/\mathcal{P}}$ is Direction Cosine Matrix (DCM) mapping from each spacecraft p fixed frame $\mathcal{P}$ to spacecraft q fixed frame $\mathcal{Q}$, and $\boldsymbol{B}_d$ is the disturbance magnetic field due to the other components and the Earth's magnetic field (assuming that the spacecraft are all in Earth orbit). Note that the magnetic field $\boldsymbol{B}_q$ may not be calculated by using Eq. (2) because of relative distance between the magnetic coils and MFS on the spacecraft q. With the configuration, the magnetic field should be expressed by Biot-savart law as

$$
{}^{\mathcal{Q}}\boldsymbol{B} = \frac{\mu_0 I N}{4\pi}\int \frac{d\boldsymbol{r}\times\left(\boldsymbol{r}_m-\boldsymbol{r}'\right)}{|\boldsymbol{r}_m-\boldsymbol{r}'|^3} \tag{10}
$$

where, I is current, N is number of turns, and $d\boldsymbol{r}$ is the infinitesimal wire segment, and $\boldsymbol{r}_m$ is position vector of MFS with respect to center of the coil, and $\boldsymbol{r}'$ is position vector of the wire segment with respect to the center of the coil.

Our proposed method estimates the relative position vector using the magnetic field modulated with a specific single-frequency. Spacecraft q segregates magnetic field ${}^{\mathcal{Q}}\boldsymbol{B}_{\mathrm{E}p}$ by using the BPF to estimate the position vector of spacecraft p. Transfer function of the BPF, $H(s)$, is expressed as follows:

$$
H(s) = \frac{O(s)}{I(s)} = \frac{(\Omega_f/Q)s}{s^2+(\Omega_f/Q)s+\Omega_f^2} \tag{11}
$$

where, Ω_f is the peak frequency, and Q is q-factor. Employing the prewarping technique, the discretized BPF by Tustin transform is expressed as

$$
o[k] = \frac{\alpha\Omega_f\left(i[k]-i[k-2]\right)+2Q\beta o[k-1]+\gamma o[k-2]}{\alpha^2 Q+\alpha\Omega_f+\Omega_f^2 Q} \tag{12}
$$

where, $\alpha=\Omega_f/\tan(\Omega_f\Delta t_s/2)$, $\beta=(\alpha^2-\Omega_f^2)$, $\gamma=\{\alpha\Omega_f-Q(\alpha^2+\Omega_f^2)\}$, and Δt_s is the sampling time.

4. Initial position estimator

4.1. Relative position vector using magnetic field and moment vectors

If the relative position between two spacecraft is unknown, it is estimated first by a Initial Position Estimator (IPE). For the IPE, relation between relative position vector and magnetic field is derived in this section.

If the segregation is successfully accomplished by the BPF, the relative position vector is calculated. The magnetic field of spacecraft p is expressed as

$$
{}^{\mathcal{P}}\boldsymbol{B}_p = \frac{\mu_0}{4\pi r_{pq}^4}\left(-\boldsymbol{M}_p r_{pq}+3M_p\boldsymbol{r}_{pq}\cos\theta\right) \tag{13}
$$

where, $M_p=||\boldsymbol{M}_p||$, $B_p=||\boldsymbol{B}_p||$, and θ is an angle between the magnetic moment vector $\boldsymbol{M}_p$ and the relative position vector $\boldsymbol{r}_{pq}$ as

$$
\theta = \cos^{-1}\left(\frac{{}^{\mathcal{P}}\boldsymbol{M}_p\cdot{}^{\mathcal{P}}\boldsymbol{r}_{pq}}{M_p r_{pq}}\right). \tag{14}
$$

The norm of the magnetic field is

$$
B_p = ||{}^{\mathcal{P}}\boldsymbol{B}_p|| = \frac{\mu_0 M_p}{4\pi r_{pq}^3}\sqrt{1+3\cos^2\theta} \tag{15}
$$

The norm of the relative position vector is derived from Eq. (15) as

$$
r_{pq} = r_{qp} = \left(\frac{\mu_0 M_p}{4\pi B_p}\zeta\right)^{1/3} \tag{16}
$$

where, $\zeta=\sqrt{1+3\cos^2\theta}$. This Eq. (16) is similarly derived in Ref. [22]. Eq. (16) insists that the range can be obtained if norms of the magnetic moment and the magnetic field by the coil are known. Thus Eq. (16) can be used for target spacecraft position estimation in a similar approach with the GPS based positioning, if at least four spacecraft can measure the target magnetic field. Substituting Eq. (16) into Eq. (13), the relative position vector is derived as:

$$
{}^{\mathcal{P}}\boldsymbol{r}_{pq} = \frac{r_{pq}}{3\cos\theta}\left({}^{\mathcal{P}}\hat{\boldsymbol{B}}_p\zeta+{}^{\mathcal{P}}\hat{\boldsymbol{M}}_p\right) \tag{17}
$$

where, $\hat{}$ indicates the unit vector. See Appendix A for the details of the analytical derivation of Eq. (16) and Eq. (17). Although Eq. (17) expresses relation between the relative position and magnetic field vectors, the equation does not hold as θ approaches to 0, for which the magnetic moment vector becomes parallel to the position vector. A solution to avoid such singularity can be using the unit direction vector instead. Noting that the position vector $\boldsymbol{r}_{pq}$ of Eq. (17) consists of two parts, which are the magnitude and the unit direction vector parts as $\boldsymbol{r}_{pq}=r_{pq}\hat{\boldsymbol{r}}_{pq}$, the singularity clearly exists in the latter. By normalizing $\hat{\boldsymbol{r}}_{pq}$, the unit vector part is expressed without the singularity as:

$$
\begin{aligned}
{}^{\mathcal{P}}\tilde{\boldsymbol{r}}_{pq} &= \frac{{}^{\mathcal{P}}\hat{\boldsymbol{r}}_{pq}}{||{}^{\mathcal{P}}\hat{\boldsymbol{r}}_{pq}||} \\
&= \frac{\frac{1}{3\cos\theta}\left({}^{\mathcal{P}}\hat{\boldsymbol{B}}_p\zeta+{}^{\mathcal{P}}\hat{\boldsymbol{M}}_p\right)}{\sqrt{\left\{\frac{1}{3\cos\theta}\left({}^{\mathcal{P}}\hat{\boldsymbol{B}}_p\zeta+{}^{\mathcal{P}}\hat{\boldsymbol{M}}_p\right)\right\}^2}} \\
&= \frac{{}^{\mathcal{P}}\hat{\boldsymbol{B}}_p\zeta+{}^{\mathcal{P}}\hat{\boldsymbol{M}}_p}{\sqrt{\left({}^{\mathcal{P}}\hat{\boldsymbol{B}}_p\zeta+{}^{\mathcal{P}}\hat{\boldsymbol{M}}_p\right)^2}}.
\end{aligned} \tag{18}
$$

Then, Eq. (17) is rewritten as

$$ {}^{\mathcal{P}}\boldsymbol{r}_{pq} = r_{pq}\ {}^{\mathcal{P}}\tilde{\boldsymbol{r}}_{pq}. \tag{19} $$

The relative position vector of spacecraft p with respect to the spacecraft q is finally expressed as:

$$ \begin{aligned} {}^{\mathcal{Q}}\boldsymbol{r}_{qp} &= \boldsymbol{R}^{\mathcal{Q}/\mathcal{P}} \cdot (-{}^{\mathcal{P}}\boldsymbol{r}_{pq}) \\ &= r_{qp}\ {}^{\mathcal{Q}}\tilde{\boldsymbol{r}}_{qp}. \end{aligned} \tag{20} $$

As a defect, the normalization causes a sign-indefinite relative position vector because of the elimination of $1/\cos\theta$ term. If only one MFS measures the magnetic field with a single-frequency, therefore, this method cannot determine the sign of the relative position vector. Even if $1/\cos\theta$ term was not eliminated, the sign ambiguity still exists since the true angle θ_{T} is unknown as long as the true position vector is not known as shown in Eq. (14). This sign ambiguity is mainly due to the fact that the magnetic field values at two locations are equal, i.e. $\boldsymbol{B}_p(\boldsymbol{r}_{pq}) = \boldsymbol{B}_p(-\boldsymbol{r}_{pq})$ as in Eq. (2). A simple solution of this sign ambiguity is to use two MFSs on all spacecraft. In this case, the distance between the two MFSs should be larger than errors of IPE. These errors of IPE are discussed in Sec. 4.2. To estimate relative position vector by the IPE, segregated magnetic field, start timing and amplitude of modulated magnetic moment are required as information to solve Eq. (20).

4.2. Sensitivity analysis for relative position depending on zeta function $\zeta(\theta)$

In the IPE process, the unknown zeta function $\zeta(\theta)$ in Eq. (16) and (20) is a problem. A solution to this problem is that $\zeta(\theta) = 1.5$ is substituted in Eq. (16) and (20), which is the intermediate value such that $1 \le \zeta(\theta) \le 2\ (\forall\theta)$ [22]. In this section, further analysis is conducted to understand the effects of the zeta function $\zeta(\theta)$ on the relative position estimation accuracy. A set of guides to preset the zeta function is discussed. Specific to this section, it is assumed that the magnetic moment and magnetic field are ideally acquired (e.g., there is no noise nor error in these values), so the actual effect of different zeta values can be evaluated.

4.2.1. Absolute position with the zeta function $\zeta(\theta)$

Introducing the subscripts T and A for true and calculated absolute positions respectively, the error e is expressed using Eq. (16) as follows:

$$ \begin{aligned} e &= r_{\mathrm{A}pq} - r_{\mathrm{T}pq} \\ &= r_{\mathrm{T}pq} \left\{ \left(\frac{\zeta_{\mathrm{A}}(\theta_{\mathrm{A}})}{\zeta_{\mathrm{T}}(\theta_{\mathrm{T}})} \right)^{1/3} - 1 \right\} \end{aligned} \tag{21} $$

See Appendix B.1 for the details of the derivation of Eq. (21). From Eq. (21), it is seen that the error depends on $\zeta_{\mathrm{A}}/\zeta_{\mathrm{T}}$. The percent of error is expressed as $e_{\%} = (e/r_{\mathrm{T}pq}) \times 100[\%]$ with respect to the true absolute position. When spacecraft p is on circular orbit around spacecraft q, the angle θ_{T} varies as $0 \le \theta_{\mathrm{T}} \le 2\pi$, which is $1 \le \zeta_{\mathrm{T}} \le 2$. If $\zeta_{\mathrm{A}} = 2$ is preset on an on-board computer of the spacecraft q, the maximum and minimum errors occur when $\zeta_{\mathrm{T}} = 1$ and $\zeta_{\mathrm{T}} = 2$, respectively. Then, the maximum and minimum errors are calculated as $e_{\max} = +0.26 r_{\mathrm{T}pq}$ and $e_{\min} = 0$. Similarly, the errors are $e_{\max} = 0$ and $e_{\min} = -0.21 r_{\mathrm{T}pq}$ when $\zeta_{\mathrm{A}} = 1$ is preset. If the $\zeta_{\mathrm{A}} = 1.44$ is preset, the error occurs in $e = \pm 0.13 r_{\mathrm{T}pq}$. These results are shown in Fig. 2. From the analysis, the ζ_A determines how the error appears. Therefore, the ζ_A can be preset suitably for each mission.

4.2.2. Position vector with the zeta function $\zeta(\theta)$

As with the absolute position, the unit position vector has also the zeta function $\zeta(\theta)$. The zeta function is defined ζ_{U} for the unit vector $\tilde{\boldsymbol{r}}_{pq}$ using Eq. (19) to distinguish from the ζ_{A} in absolute position calculation. Defining calculated position vector $\boldsymbol{r}_{\mathrm{C}pq} = r_{\mathrm{A}pq}(\zeta_{\mathrm{A}})\boldsymbol{r}_{\mathrm{U}pq}(\zeta_{\mathrm{U}})$ to distinguish from the true position vector, the error for the calculated position vector $\boldsymbol{e}$ is expressed as follows:

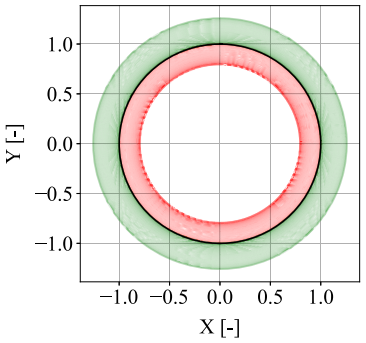

Fig. 2. Calculated absolute position on true orbital plane: True orbit is black solid line, green region is absolute position calculated with $\zeta_{\mathrm{A}} = 2$, and red region is absolute position calculated with $\zeta_{\mathrm{A}} = 1$. (For interpretation of the colors in the figure(s), the reader is referred to the web version of this article.)

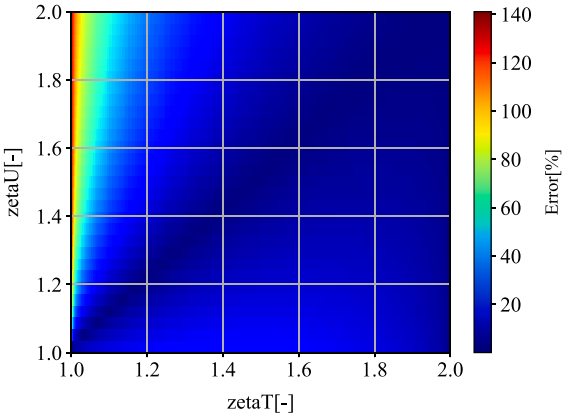

Fig. 3. Absolute error of calculated position vector depending on zeta functions ζ_{T} and ζ_{U}.

$$ \begin{aligned} \boldsymbol{e} &= \boldsymbol{r}_{\mathrm{C}pq}(\zeta_{\mathrm{A}}, \zeta_{\mathrm{U}}) - \boldsymbol{r}_{\mathrm{T}pq}(\zeta_{\mathrm{T}}) \\ &= r_{\mathrm{T}pq}\zeta_{\mathrm{T}}\Lambda_{\mathrm{B}} \frac{\hat{\boldsymbol{B}}_p}{||\hat{\boldsymbol{r}}_{\mathrm{T}pq}||} + r_{\mathrm{T}pq}\Lambda_{\mathrm{M}} \frac{\hat{\boldsymbol{M}}_p}{||\hat{\boldsymbol{r}}_{\mathrm{T}pq}||} \\ &= r_{\mathrm{T}pq} \left(\zeta_{\mathrm{T}}\Lambda_{\mathrm{B}} \frac{\hat{\boldsymbol{B}}_p}{||\hat{\boldsymbol{r}}_{\mathrm{T}pq}||} + \Lambda_{\mathrm{M}} \frac{\hat{\boldsymbol{M}}_p}{||\hat{\boldsymbol{r}}_{\mathrm{T}pq}||} \right) \end{aligned} \tag{22} $$

where,

$$ \Lambda_{\mathrm{B}} = \frac{||\hat{\boldsymbol{r}}_{\mathrm{T}pq}||}{||\hat{\boldsymbol{r}}_{\mathrm{U}pq}||} \frac{\zeta_{\mathrm{U}}}{\zeta_{\mathrm{T}}} \frac{r_{\mathrm{A}pq}}{r_{\mathrm{T}pq}} - 1 \tag{23} $$

and

$$ \Lambda_{\mathrm{M}} = \frac{||\hat{\boldsymbol{r}}_{\mathrm{T}pq}||}{||\hat{\boldsymbol{r}}_{\mathrm{U}pq}||} \frac{r_{\mathrm{A}pq}}{r_{\mathrm{T}pq}} - 1 \tag{24} $$

See Appendix B.2 for the details of the derivation of the above error expression. Although the analytical expression of error is complex, Eq. (22) gives a way to determine the ζ_{U}. The absolute value of error $\boldsymbol{e}$ depending on the ζ_{U} and ζ_{T} is shown in Fig. 3. As seen in Fig. 3, large error occurs when $\zeta_{\mathrm{T}} \to 1$ ($\theta_{\mathrm{T}} \to \pi/2$) because the magnetic field vectors are measured as equal on plane perpendicular to magnetic moment vector, which $\theta_{\mathrm{T}} = \pi/2$. Therefore, this proposed method does not work in the case that MFS is completely on the plane. The error for $\zeta_{\mathrm{T}} = 1$ reaches to minimum when both $\zeta_{\mathrm{T}} = \zeta_{\mathrm{U}} = 1$. From the results, the zeta function ζ_{U} should be preset as $\zeta_{\mathrm{U}} = 1$ although $1 \le \zeta_{\mathrm{A}} \le 2$. The process of IPE is summarized in Algorithm 1.

4.2.3. A method to update $\zeta(\theta)$ for accurate initial position estimation

Even if the initial position vector that is calculated using Eq. (20) is a rough estimate, the UKF that is used next minimizes the errors. How-

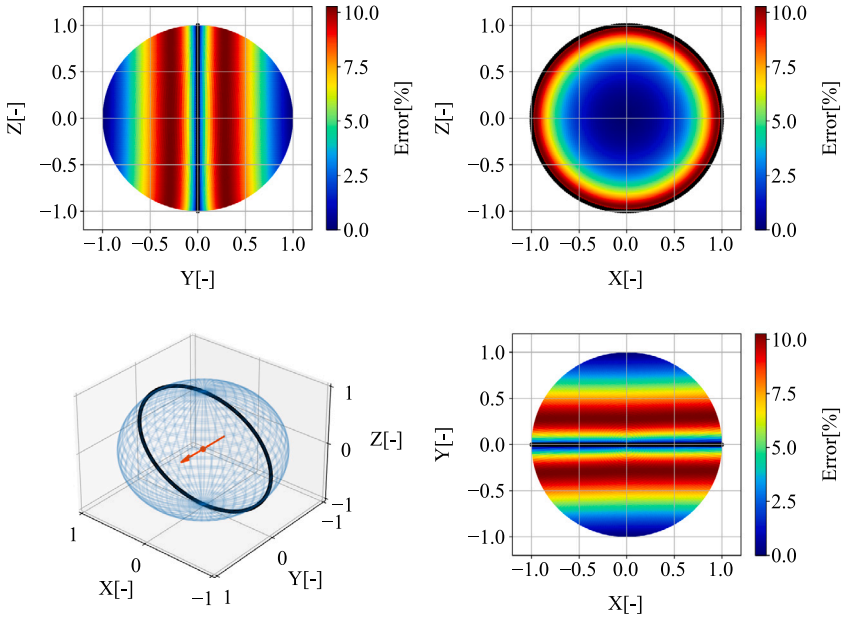

Fig. 4. Absolute error of calculated position vector with updated ζ'_{T} with $\zeta_{\mathrm{A}} = 1.44$ and $\zeta_{\mathrm{U}} = 1.0$: (X-Z plane: top right), (Y-Z plane: top left), (X-Y plane: bottom right), (relation between spacecraft p (orange dot) and position of spacecraft q (Blue lines): bottom left).

ever, large initial errors make the UKF converge in long time and the sign ambiguity may not be solved quickly even if two MFSs are used. To reduce the calculation error, ζ_{A} and ζ_{U} can be updated with a better estimate as ζ'_{T}. The ζ'_{T} is estimated by using the calculated position vector, which the IPE outputs in the first iteration ${}^{\mathcal{Q}}\boldsymbol{r}_{Cqp}$, and the magnetic moment vector ${}^{\mathcal{Q}}\boldsymbol{M}_p$ by using Eq. (14) as

$$\zeta'_{\mathrm{T}} = \sqrt{1 + 3\left(\frac{{}^{\mathcal{Q}}\boldsymbol{M}_p \cdot {}^{\mathcal{Q}}\boldsymbol{r}_{Cqp}}{M_p r_{Cqp}}\right)^2} \tag{25}$$

This process corresponds to line 9 ∼ line 11 in Algorithm 1. Assuming that the magnetic moment vector and the magnetic field vector can be acquired ideally, absolute error for the calculated position vector with ζ'_{T} as $||\boldsymbol{r}_{\mathrm{C}pq} - \boldsymbol{r}_{\mathrm{T}pq}||$ occurs as shown in Fig. 4. The unit magnetic moment vector is $\hat{\boldsymbol{M}}_p = [0, 1, 0]^T$ shown as an arrow in Fig. 4 (bottom right). The black line in Fig. 4 shows the location where the proposed method does not work because the magnetic field vectors within the plane perpendicular to the magnetic moment vector of the spacecraft p are equal. As seen in Fig. 4, ±10.2[%] error should be taken into account as the maximum in the IPE process using Eq. (19) with the updated zeta function, which the preset zeta functions are $\zeta_{\mathrm{A}} = 1.44$ and $\zeta_{\mathrm{U}} = 1.0$. In actual operation, this error in the initial position estimate will be larger due to the magnetic sensor errors and other factors, which are not accounted in this section. Thus the estimate by the IPE for the relative position must be refined using the UKF.

5. Sequential position estimator using the unscented Kalman filter

Once the initial relative position is estimated, an Unscented Kalman Filter (UKF) is run for sequential position estimation. Nonlinear state and observation equations are given as follows:

$$\begin{cases} \dot{\boldsymbol{X}} = \boldsymbol{f}(\boldsymbol{X}, \boldsymbol{u}) + \boldsymbol{w}_r \\ \boldsymbol{Y} = \boldsymbol{h}(\boldsymbol{X}, \boldsymbol{w}_b) \end{cases} \tag{26}$$

where, $\boldsymbol{X} \in \mathbb{R}^n$ and $\boldsymbol{Y} \in \mathbb{R}^m$ are states and measurements. The process noise $\boldsymbol{w}_r \sim \boldsymbol{N}(0, \sigma_r^2)$ and measurement noise $\boldsymbol{w}_b \sim \boldsymbol{N}(0, \sigma_b^2)$ are white Gaussian noise with covariances σ_r^2 and σ_b^2 respectively. The functions

Algorithm 1 Algorithm for initial position estimation.

Input: Magnetic field ${}^{\mathcal{Q}}\boldsymbol{B}_{\mathrm{TOT}}$, Magnetic dipole vector ${}^{\mathcal{P}}\boldsymbol{M}_p$, and DCM $\boldsymbol{R}^{\mathcal{Q}/\mathcal{P}}$
Output: Relative position vector ${}^{\mathcal{Q}}\boldsymbol{r}_{Cqp}$
Initialisation :
1: Set ζ_{A} to $1.0 \sim 2.0$ and $\zeta_{\mathrm{U}} = 1.0$
OBC process :
2: Segregate target magnetic field ${}^{\mathcal{Q}}\boldsymbol{B}_p(\omega_p)$ from ${}^{\mathcal{Q}}\boldsymbol{B}_{\mathrm{TOT}}$ using BPF according to Eq. (12)
3: **if** ${}^{\mathcal{Q}}\boldsymbol{B}_p(\omega_p) \geq \boldsymbol{w}_b$ **then**
4: Compute ${}^{\mathcal{Q}}\boldsymbol{M}_p = \boldsymbol{R}^{\mathcal{Q}/\mathcal{P}} \cdot {}^{\mathcal{P}}\boldsymbol{M}_p$
5: Compute $B_p = ||{}^{\mathcal{Q}}\boldsymbol{B}_p(\omega_p)||$
6: Compute $M_p = ||{}^{\mathcal{Q}}\boldsymbol{M}_p||$
7: Compute r_{qp} according to Eq. (16) using ζ_{A}
8: Compute ${}^{\mathcal{Q}}\boldsymbol{r}_{qp}$ according to Eq. (20) using ζ_{A} and ζ_{U}
9: Compute ζ'_{T} according to Eq. (25)
10: Update $\zeta_{\mathrm{A}} \leftarrow \zeta'_{\mathrm{T}}$ and $\zeta_{\mathrm{U}} \leftarrow \zeta'_{\mathrm{T}}$
11: Compute ${}^{\mathcal{Q}}\boldsymbol{r}_{qp}$ according to Eq. (20)
12: **else**
13: ${}^{\mathcal{Q}}\boldsymbol{r}_{qp} = \mathrm{NaN}$
14: **end if**
15: **return** ${}^{\mathcal{Q}}\boldsymbol{r}_{qp}$

Algorithm 2 Algorithm for sequential position estimation.

Input: Initial relative state vector ${}^{\mathcal{Q}}\boldsymbol{X}_0 = {}^{\mathcal{Q}}[\boldsymbol{r}_{qp}, \boldsymbol{v}_{qp0}]$, where $\boldsymbol{v}_{qp0} = \boldsymbol{0}$, and covariance matrix $\boldsymbol{P}_0$, ${}^{\mathcal{Q}}\boldsymbol{B}_{\mathrm{TOT}}$
Output: ${}^{\mathcal{Q}}\tilde{\boldsymbol{X}}$
Initialisation :
1: Generate sigma points $\boldsymbol{\mathcal{X}} = \left[\chi_0, \chi_{i\in\{1,2,3\ldots 2n\}}\right]$
2: Calculate weights W_i
Begin :
3: Process *time update* of predicted states
4: Update sigma points
5: Process *time update* of predicted observation
6: Segregate target magnetic field modulated ${}^{\mathcal{Q}}\boldsymbol{B}_p(\omega_p)$ from ${}^{\mathcal{Q}}\boldsymbol{B}_{\mathrm{TOT}}$ using BPF according to Eq. (12)
7: Update ${}^{\mathcal{Q}}\tilde{\boldsymbol{X}}$ by *observation update*
8: **return** ${}^{\mathcal{Q}}\tilde{\boldsymbol{X}}$

$f : \mathbb{R}^n \to \mathbb{R}^n$ and $h : \mathbb{R}^n \to \mathbb{R}^m$ represent nonlinear dynamics and observation models. Employing Hill-Clohessy-Wiltshire (HCW) equation [27],

Table 1
Numerical simulation condition.

	Parameter	Value
Orbit	Altitude [km]	500
OBC	Clock frequency [Hz]	10
BPF	Q factor [-]	35
STT	Mean [arcsec]	0
	SD[arcsec]	30
	Sampling frequency [Hz]	2.0
MFS	Mean [nT]	0
	SD [nT]	100
	Sampling frequency [Hz]	10
Coil	Radius [m]	0.1
	Height [m]	0.1
	Turn number [-]	3000
	Magnetic moment [Am^2]	$[0, 10, 0]^T$
	Frequency of spacecraft q [Hz]	1.0
	Frequency of spacecraft 1 [Hz]	0.5
	Frequency of spacecraft 2 [Hz]	1.5
	Frequency of spacecraft 3 [Hz]	2.0
	Frequency of spacecraft 4 [Hz]	2.5

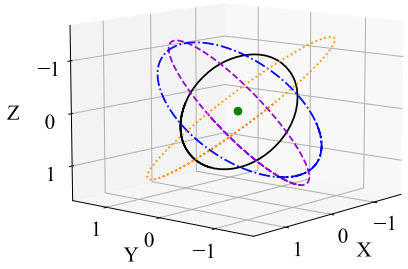

Fig. 5. Spacecraft orbits with respect to the spacecraft q: Black solid line, purple dashed line, blue dot-dashed line, and orange dots line indicate orbits of spacecraft 1, 2, 3, and 4 respectively. Green dot is the location of spacecraft q.

the relative orbit dynamics of spacecraft p with respect to spacecraft q is expressed as:

$$ {}^{\mathcal{Q}}\boldsymbol{f}(\boldsymbol{X},\boldsymbol{u}) = \begin{cases} \ddot{x} &= 3n^2x + 2n\dot{y} + u_x \\ \ddot{y} &= -2n\dot{x} + u_y \\ \ddot{z} &= -n^2z + u_z \end{cases} \tag{27} $$

where, a relative state vector is ${}^{\mathcal{Q}}\boldsymbol{X} = {}^{\mathcal{Q}}[\boldsymbol{r}_{qp}, \boldsymbol{v}_{qp}]^T$, $n = \sqrt{\mu_0/R^3}$ represents angular rate of circular orbits around the Earth with the radius of R, and ${}^{\mathcal{Q}}\boldsymbol{u} = [u_x, u_y, u_z]^T$ is input force. If the orbits are not circular, the other orbit model such as Yamanaka-Ankerson's equation [28] should be applied. The observation equation is given as

$$ {}^{\mathcal{Q}}\boldsymbol{h}\left(\boldsymbol{X}, \boldsymbol{w}_b\right) = \boldsymbol{R}^{\mathcal{Q}/\mathcal{P}}(\boldsymbol{\theta} + \boldsymbol{w}_{b1}) \cdot {}^{\mathcal{P}}\boldsymbol{B}_p\left({}^{\mathcal{P}}\boldsymbol{M}_p, {}^{\mathcal{P}}\boldsymbol{r}_{pq}\right) + \boldsymbol{w}_{b2} \tag{28} $$

where, $\boldsymbol{\theta}$ is relative attitude between $\mathcal{P}$ and $\mathcal{Q}$, $\boldsymbol{w}_{b1}$ and $\boldsymbol{w}_{b2}$ are the noise of the attitude sensor and the MFS respectively. The algorithm of sequential relative position estimation is shown in Algorithm 2. Reader may refer to [29] for standard UKF formulation.

6. Conditions for using the proposed method

The proposed method mainly consists of two parts, which are the IPE and the UKF. Following requirements must be fulfilled to use the proposed IPE and UKF.

1. Spacecraft in the formation must have a Star Tracker (STT), two MFSs, and magnetic coils at least.
2. Spacecraft in the formation can drive magnetic coils with an assigned frequency, direction and amplitude for the position vector estimation.

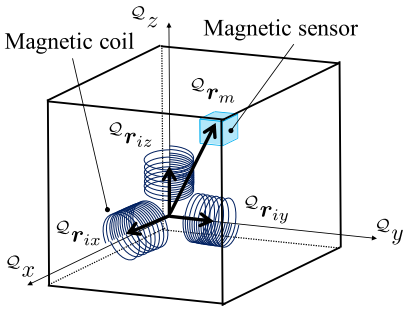

Fig. 6. Spacecraft configuration in the numerical simulations.

3. Nyquist frequency of MFS should be greater than AC magnetic field for the position estimation. If the Nyquist frequency is below the magnetic field for controlling, an anti-aliasing filter should be applied.
4. On-Board Computer (OBC) clocks of all spacecraft in the formation are synchronized. Moreover, the spacecraft can adjust the timing of AC magnetic field using the established communication link.
5. Measured magnetic field must be larger than the sensor noise. Otherwise, BPF cannot segregate the target AC magnetic field, especially for the IPE (see line 3 in Algorithm 1).
6. Relative attitude is known (for example, using the established communication link).

7. Numerical simulation

To validate the IPE and UKF, numerical simulations are conducted and the results are shown in this section. In the numerical simulations, we consider four spacecraft $p \in \{1, 2, 3, 4\}$ are flying nearby the spacecraft q as shown in Fig. 5. Spacecraft have STT and MFSs, and drive their coils with the details given in Table 1. The spacecraft q attempts to estimate the relative position vector of spacecraft 1 in this simulation. It is assumed that all spacecraft control to maintain their attitude with respect to inertial frame. The magnetic field generated by coils on the spacecraft q itself is calculated by using Eq. (10) with the configuration as shown in Fig. 6. Spacecraft are 0.5 m cubes and MFS is located at ${}^{\mathcal{Q}}\boldsymbol{r}_m = [0.4, 0.4, 0.4]^T$ m with respect to the spacecraft frame. In this simulation, it is assumed that sign ambiguity is solved by using two MFSs. If the sign ambiguity is solved using some another technique, the relative position vector can be estimated by using only one MFS. Normal vectors of magnetic coils that are placed orthogonally are along the basis vectors of the spacecraft fixed frame. Centers of magnetic coils are located at $\boldsymbol{r}_{ix} = [0.25, 0, 0]^T$ m, $\boldsymbol{r}_{iy} = [0, 0.25, 0]^T$ m, and $\boldsymbol{r}_{iz} = [0, 0, 0.25]^T$ m, respectively. In addition, the MFS on the spacecraft q measures also the Earth magnetic field, which is approximated with a magnetic dipole model whose magnitude is 8.0×10^{22}Am^2.

7.1. Results for initial position estimation

Applying the Algorithm 1 for initial relative position estimation, results of the estimation are shown in Fig. 7. This method enables estimating the relative position vector of the spacecraft 1. IPE outputs relative position vector indicating red dots in the Fig. 7. Considering errors between the true orbit and the estimated position, the maximum estimation errors are $\Delta\boldsymbol{r}_{qp} = [-17.4 \times 10^{-2}, -18.1 \times 10^{-2}, -16.5 \times 10^{-2}]^T$ m as shown in Fig. 8. Results show that the IPE can estimate the relative position vector with errors approximately ± 0.18 m for this simulation condition. Although the error is large for the EMFF, the IPE enables to estimate the relative position vector. The shaded region indicates where the IPE can not determine the relative position vector due to small amplitude of magnetic field buried in the sensor noise mentioned in Sec. 6. In this numerical simulation, all spacecraft modulate and control their magnetic moment along y axis with respect to the spacecraft q fixed

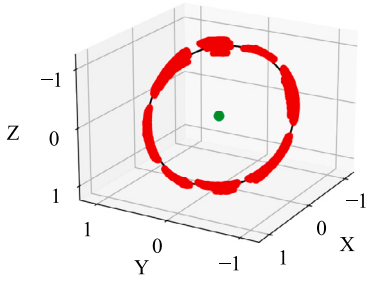

Fig. 7. Result for the initial position estimation in half of an orbit: True orbit is black solid line, red dots are the estimated positions, and green dot indicates the spacecraft p.

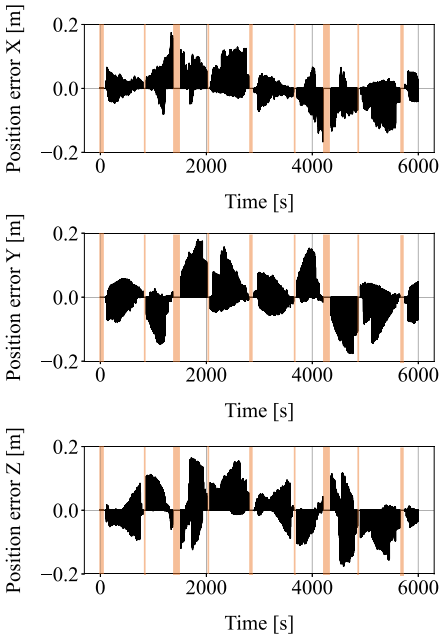

Fig. 8. Position estimation errors of the initial position estimation method in one orbit: the estimation error is black solid lines of each axis with respect to spacecraft q fixed frame, and orange shaded region is locations where the amplitude of magnetic field is lower than the noise of MFS.

Table 2
Parameters of UKF.

Parameter	Value
Initial position error σ_{p0}^2 $[m^2]$	1.8×10^{-2}
Initial velocity error σ_{v0}^2 $[m^2/s^2]$	7.2×10^{-7}
Position error σ_p^2 $[m^2]$	2.7×10^{-4}
Velocity error σ_v^2 $[m^2/s^2]$	8.0×10^{-8}
Observation error σ_m^2 $[T^2]$	1.0×10^{-12}
Initial matrix $\boldsymbol{P}_0$	$\mathrm{diag}\left(\sigma_{p0}^2,\sigma_{p0}^2,\sigma_{p0}^2,\sigma_{v0}^2,\sigma_{v0}^2,\sigma_{v0}^2\right)$
The process noise $\boldsymbol{Q}$	$\mathrm{diag}\left(\sigma_p^2,\sigma_p^2,\sigma_p^2,\sigma_v^2,\sigma_v^2,\sigma_v^2\right)$
The observation noise $\boldsymbol{R}$	$\mathrm{diag}\left(\sigma_m^2,\sigma_m^2,\sigma_m^2\right)$

frame as in Table 1. After the IPE finds the vectors, the UKF runs for sequential position estimation. Applying the UKF, the proposed method estimates relative position vectors sequentially.

7.2. Results of sequential position estimation

From the estimated initial position vector in the IPE, the spacecraft q attempts to reduce the estimation error and estimate the relative position sequentially using the UKF. In this numerical simulation, it is assumed that the spacecraft q successes to estimate the initial position vector with the errors $\Delta\boldsymbol{r}_{qp}$ by using the IPE. The parameters of UKF are shown in Table 2. Applying Algorithm 2, the UKF reduces the errors of the IPE in 200 seconds as shown in Fig. 9. The UKF can estimate the relative orbit velocities as in Fig. 9 as well. Mean Errors (ME) of the estimated relative position in one orbit after the 200 seconds are calculated as $[6.29\times10^{-4}, -6.06\times10^{-4}, 4.64\times10^{-4}]^T$ m and MEs of the estimated velocity are$[5.76\times10^{-7}, -7.48\times10^{-7}, 1.88\times10^{-7}]^T$ m/s. In addition, the Standard Error of the Mean (SEM(1σ)) of the estimated relative position after the 200 seconds is $[9.08\times10^{-3}, 17.6\times10^{-3}, 18.3\times10^{-3}]^T$ m and SEM(1σ) of the estimated velocity is $[2.04\times10^{-5}, 3.17\times10^{-5}, 2.67\times10^{-5}]^T$ m/s respectively. Compared to the IPE, the UKF can estimate the relative position vector more accurately. As seen in Fig. 9, covariances degrade at some locations because the BPF cannot segregate the target magnetic field due to low amplitude of the magnetic field. However, the UKF achieves errors smaller than $\pm3.56\times10^{-2}$ m, which is the maximum error of Z axis, in the position estimation for all axes. Thus, the UKF can reduce the estimation error of IPE and estimate sequentially the relative position vector even if BPF cannot segregate the target magnetic field correctly. To confirm the performance of the UKF, Monte Carlo simulations are conducted. In the Monte Carlo simulations, the initial position errors are uniformly distributed in the range of ±0.5 m. Averaged results for the Monte Carlo analysis with repeated 300 UKF runs are shown in Table 3. The estimation results converge to the actual values with errors shown in Table 3 even if large estimation errors for the IPE are observed. If the initial position vector is provided to the UKF, therefore, the relative position vector can be estimated within 5.43×10^{-2} m error (3σ). Results clearly indicate that the proposed method is a potentially new solution for relative position estimation which can provide centimeter level accuracy.

Table 3
Averaged ME and SEM of the UKF from the Monte Carlo simulation (300 runs).

	ME	SEM(1σ)
Position error of X [m]	2.64×10^{-4}	1.03×10^{-2}
Position error of Y [m]	-1.61×10^{-4}	1.77×10^{-2}
Position error of Z [m]	5.54×10^{-4}	1.81×10^{-2}
Velocity error of X [m/s]	1.82×10^{-7}	3.05×10^{-5}
Velocity error of Y [m/s]	-4.01×10^{-7}	3.28×10^{-5}
Velocity error of Z [m/s]	5.76×10^{-7}	3.44×10^{-5}

The proposed method can find the target position vector even if the relative position is unknown. This is the advantage of the proposed method in comparison to the laser range finder, vision-based method, and the approach in [20]. Although our proposed method requires spacecraft to establish a communication link with the target, only one link is enough to estimate the relative position, which is dynamically changing by relative orbital motion. As shown in the numerical results, however, the accuracy of this proposed method is at a centimeter level, although the other methods can achieve millimeter-level accuracy. If users require higher estimation accuracy of the proposed method, measurement accuracy and sampling frequency of MFSs and OBC clock frequencies shown in Table 1 should mainly be improved. Based on our experience of numerical simulation, OBC with more than 10 Hz clock frequency should be applied for stable convergence of UKF from errors of IPE. It is especially recommended that the sampling frequency is four times more than the modulation frequency of targets. If the undesired magnetic field by components on spacecraft affects the estimation accuracy of the proposed method, placing the MFSs at a distance using booms is one of the solutions.

8. Conclusion

The relative position estimation method by using AC magnetic field is proposed in this paper. The proposed method consists of two parts,

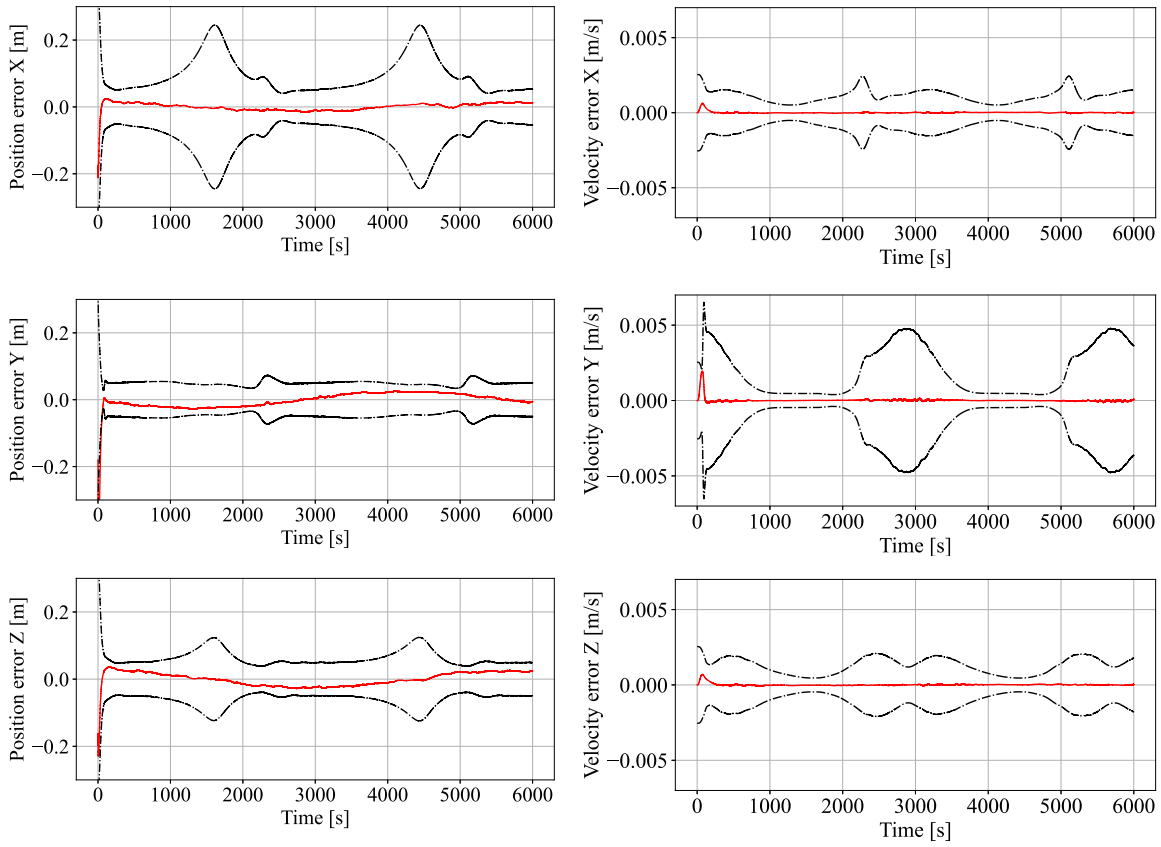

Fig. 9. Position estimation errors by the sequential position estimation method: red solid-line indicates estimation error of position and velocity, and black dot-dashed line indicates 3σ standard deviation.

which are initial and sequential estimators. Compared with other methods such as those using the laser range finders and image sensors, the proposed method does not require attitude control to track target spacecraft. Measuring the magnetic field and establishing a communication link to acquire relative attitude information are sufficient. Performance of this proposed method is evaluated by the numerical simulations. Position vectors of spacecraft in formation are initially estimated by the IPE. Although this initial method contains relatively large errors, which is few tens of centimeters in the condition of the conducted numerical simulations, it enables finding the target spacecraft using only magnetic field and attitude information. Once the initial relative position vector is estimated, the UKF runs to estimate the position more accurately. The results of Monte Calro simulation show that the UKF can converge even if the IPE has large errors. Using this proposed method, relative position vector between spacecraft in the formation can be estimated even when it changes dynamically due to the relative orbital motion.

CRediT authorship contribution statement

Takuma Shibata: Writing – original draft, Validation, Software. **Halil Ersin Söken:** Writing – review & editing, Validation, Supervision. **Shin-ichiro Sakai:** Writing – review & editing, Validation, Supervision.

Declaration of competing interest

The authors declare that they have no known competing financial interests or personal relationships that could have appeared to influence the work reported in this paper.

Data availability

The data that has been used is confidential.

Appendix A. Relative position vector derived from magnetic field

Dipole magnetic field is expressed as following:

$$\begin{aligned}\boldsymbol{B} &= \frac{\mu_0}{4\pi r^3}\left\{-\boldsymbol{M} + \frac{3(\boldsymbol{M}\cdot\boldsymbol{r})}{r^2}\boldsymbol{r}\right\} \\ &= \frac{\mu_0}{4\pi r^3}\left(-\boldsymbol{M} + \frac{3Mr\cos\theta}{r^2}\boldsymbol{r}\right) \\ &= \frac{\mu_0}{4\pi r^4}\left(-\boldsymbol{M}r + 3M\boldsymbol{r}\cos\theta\right)\end{aligned} \tag{A.1}$$

Then, the absolute magnetic field is derived as following:

$$\begin{aligned}B &= \sqrt{\boldsymbol{B}^T\cdot\boldsymbol{B}} \\ &= \frac{\mu_0}{4\pi r^4}\sqrt{(\boldsymbol{M}^T\cdot\boldsymbol{M})r^2 - 6Mr\cos\theta(\boldsymbol{M}^T\cdot\boldsymbol{r}) + 9M^2\cos^2\theta(\boldsymbol{r}^T\cdot\boldsymbol{r})} \\ &= \frac{\mu_0}{4\pi r^4}\sqrt{M^2r^2 - 6M^2r^2\cos^2\theta + 9M^2r^2\cos^2\theta} \\ &= \frac{\mu_0}{4\pi r^4}\sqrt{M^2r^2 + 3M^2r^2\cos^2\theta} \\ &= \frac{\mu_0 M}{4\pi r^3}\sqrt{1+3\cos^2\theta}\end{aligned} \tag{A.2}$$

Finally, the absolute position is

$$\begin{aligned}r &= \left(\frac{\mu_0 M}{4\pi B}\sqrt{1+3\cos^2\theta}\right)^{1/3} \\ &= \left(\frac{\mu_0 M}{4\pi B}\zeta\right)^{1/3}\end{aligned} \tag{A.3}$$

where, $\zeta = \sqrt{1+3\cos^2\theta}$. Substituting Eq. (A.3) into Eq. (A.1), the magnetic field vector is expressed as follows:

$$\boldsymbol{B} = \frac{B}{M\zeta}\left\{-\boldsymbol{M} + \frac{3M\cos\theta}{r}\boldsymbol{r}\right\} \tag{A.4}$$

The position vector is expressed from Eq. (A.4) as follows:

$$\begin{aligned}\boldsymbol{r} &= \frac{r}{3M\cos\theta}\left\{\frac{M\zeta}{B}\boldsymbol{B} + \boldsymbol{M}\right\} \\ &= \frac{r}{3\cos\theta}\left\{\frac{\boldsymbol{B}}{B}\zeta + \frac{\boldsymbol{M}}{M}\right\} \\ &= \frac{r}{3\cos\theta}\left\{\hat{\boldsymbol{B}}\zeta + \hat{\boldsymbol{M}}\right\}\end{aligned} \tag{A.5}$$

Appendix B. Errors of position calculation

B.1. Error of absolute position calculation

Error of absolute position is expressed using Eq. (16) as

$$\begin{aligned}e &= r_{\mathrm{A}pq} - r_{\mathrm{T}pq} \\ &= \left(\frac{\mu_0 M_p}{4\pi B_p}\zeta_{\mathrm{A}}\right)^{1/3} - \left(\frac{\mu_0 M_p}{4\pi B_p}\zeta_{\mathrm{T}}\right)^{1/3} \\ &= \left(\frac{\mu_0 M_p}{4\pi B_p}\right)^{1/3}\zeta_{\mathrm{A}}^{1/3} - \left(\frac{\mu_0 M_p}{4\pi B_p}\right)^{1/3}\zeta_{\mathrm{T}}^{1/3} \\ &= \left(\frac{\mu_0 M_p}{4\pi B_p}\right)^{1/3}\left(\zeta_{\mathrm{A}}^{1/3} - \zeta_{\mathrm{T}}^{1/3}\right)\end{aligned} \tag{B.1}$$

From Eq. (16), M_p/B_p is expressed as

$$\frac{M_p}{B_p} = \frac{4\pi r_{\mathrm{T}pq}^3}{\mu_0\zeta_{\mathrm{T}}} \tag{B.2}$$

Substituting Eq. (B.2) into Eq. (B.1), the error is rewritten as

$$\begin{aligned}e &= \left(\frac{\mu_0}{4\pi}\frac{4\pi r_{\mathrm{T}pq}^3}{\mu_0\zeta_{\mathrm{T}}}\right)^{1/3}(\zeta_{\mathrm{A}}^{1/3} - \zeta_{\mathrm{T}}^{1/3}) \\ &= r_{\mathrm{T}pq}\left\{\left(\frac{\zeta_{\mathrm{A}}}{\zeta_{\mathrm{T}}}\right)^{1/3} - 1\right\}\end{aligned} \tag{B.3}$$

B.2. Error of position vector calculation

Assuming that the magnetic dipole is correctly modeled, which $\hat{\boldsymbol{M}}_p = \hat{\boldsymbol{M}}_{\mathrm{C}p} = \hat{\boldsymbol{M}}_{\mathrm{T}p}$, the error of position vector calculation $\boldsymbol{e}$ is derived in this section. With an measured error and true magnetic field, measured magnetic field $\boldsymbol{B}_{\mathrm{C}p}$ is expressed Using Eq. (18), Eq. (19) and Eq. (B.3), error of position vector is expressed as

$$\begin{aligned}\boldsymbol{e} &= r_{\mathrm{A}pq}\tilde{\boldsymbol{r}}_{\mathrm{U}pq} - r_{\mathrm{T}pq}\tilde{\boldsymbol{r}}_{\mathrm{T}pq} \\ &= r_{\mathrm{A}pq}\frac{\hat{\boldsymbol{B}}_{\mathrm{U}p}\zeta_{\mathrm{U}} + \hat{\boldsymbol{M}}_p}{||\hat{\boldsymbol{r}}_{\mathrm{U}pq}||} - r_{\mathrm{T}pq}\frac{\hat{\boldsymbol{B}}_{\mathrm{T}p}\zeta_{\mathrm{T}} + \hat{\boldsymbol{M}}_p}{||\hat{\boldsymbol{r}}_{\mathrm{T}pq}||} \\ &= r_{\mathrm{A}pq}\zeta_{\mathrm{U}}\frac{\hat{\boldsymbol{B}}_p}{||\hat{\boldsymbol{r}}_{\mathrm{U}pq}||} - r_{\mathrm{T}pq}\zeta_{\mathrm{T}}\frac{\hat{\boldsymbol{B}}_p}{||\hat{\boldsymbol{r}}_{\mathrm{T}pq}||} + r_{\mathrm{A}pq}\frac{\hat{\boldsymbol{M}}_p}{||\hat{\boldsymbol{r}}_{\mathrm{U}pq}||} - r_{\mathrm{T}pq}\frac{\hat{\boldsymbol{M}}_p}{||\hat{\boldsymbol{r}}_{\mathrm{T}pq}||} \\ &= r_{\mathrm{A}pq}\zeta_{\mathrm{U}}\frac{\hat{\boldsymbol{B}}_p||\hat{\boldsymbol{r}}_{\mathrm{T}pq}||}{||\hat{\boldsymbol{r}}_{\mathrm{U}pq}||||\hat{\boldsymbol{r}}_{\mathrm{T}pq}||} - r_{\mathrm{T}pq}\zeta_{\mathrm{T}}\frac{\hat{\boldsymbol{B}}_p||\hat{\boldsymbol{r}}_{\mathrm{U}pq}||}{||\hat{\boldsymbol{r}}_{\mathrm{U}pq}||||\hat{\boldsymbol{r}}_{\mathrm{T}pq}||} \\ &\quad + r_{\mathrm{A}pq}\frac{\hat{\boldsymbol{M}}_p||\hat{\boldsymbol{r}}_{\mathrm{T}pq}||}{||\hat{\boldsymbol{r}}_{\mathrm{U}pq}||||\hat{\boldsymbol{r}}_{\mathrm{T}pq}||} - r_{\mathrm{T}pq}\frac{\hat{\boldsymbol{M}}_p||\hat{\boldsymbol{r}}_{\mathrm{U}pq}||}{||\hat{\boldsymbol{r}}_{\mathrm{U}pq}||||\hat{\boldsymbol{r}}_{\mathrm{T}pq}||} \\ &= (r_{\mathrm{A}pq}\zeta_{\mathrm{U}}||\hat{\boldsymbol{r}}_{\mathrm{T}pq}|| - r_{\mathrm{T}pq}\zeta_{\mathrm{T}}||\hat{\boldsymbol{r}}_{\mathrm{U}pq}||)\frac{\hat{\boldsymbol{B}}_p}{||\hat{\boldsymbol{r}}_{\mathrm{U}pq}||||\hat{\boldsymbol{r}}_{\mathrm{T}pq}||} \\ &\quad + (r_{\mathrm{A}pq}||\hat{\boldsymbol{r}}_{\mathrm{T}pq}|| - r_{\mathrm{T}pq}||\hat{\boldsymbol{r}}_{\mathrm{U}pq}||)\frac{\hat{\boldsymbol{M}}_p}{||\hat{\boldsymbol{r}}_{\mathrm{U}pq}||||\hat{\boldsymbol{r}}_{\mathrm{T}pq}||} \\ &= r_{\mathrm{T}pq}\zeta_{\mathrm{T}}\left(\frac{||\hat{\boldsymbol{r}}_{\mathrm{T}pq}||}{||\hat{\boldsymbol{r}}_{\mathrm{U}pq}||}\frac{\zeta_{\mathrm{U}}}{\zeta_{\mathrm{T}}}\frac{r_{\mathrm{A}pq}}{r_{\mathrm{T}pq}} - 1\right)\frac{\hat{\boldsymbol{B}}_p}{||\hat{\boldsymbol{r}}_{\mathrm{T}pq}||} \\ &\quad + r_{\mathrm{T}pq}\left(\frac{||\hat{\boldsymbol{r}}_{\mathrm{T}pq}||}{||\hat{\boldsymbol{r}}_{\mathrm{U}pq}||}\frac{r_{\mathrm{A}pq}}{r_{\mathrm{T}pq}} - 1\right)\frac{\hat{\boldsymbol{M}}_p}{||\hat{\boldsymbol{r}}_{\mathrm{T}pq}||}\end{aligned} \tag{B.4}$$

References

[1] Z. Kang, B. Tapley, S. Bettadpur, J. Ries, P. Nagel, Precise orbit determination for grace using accelerometer data, Adv. Space Res. 38 (2006) 2131–2136, https://doi.org/10.1016/j.asr.2006.02.021.

[2] J. Hinderer, O. Andersen, F. Lemoine, D. Crossley, J.-P. Boy, Seasonal changes in the European gravity field from grace: a comparison with superconducting gravimeters and hydrology model predictions, J. Geodyn. 41 (2006) 59–68, https://doi.org/10.1016/j.jog.2005.08.037.

[3] B. Klinger, O. Baur, T. Mayer-Gürr, Grail gravity field recovery based on the short-arc integral equation technique: simulation studies and first real data results, Planet. Space Sci. 91 (2014) 83–90, https://doi.org/10.1016/j.pss.2013.12.001.

[4] G. Krieger, M. Zink, M. Bachmann, B. Bräutigam, D. Schulze, M. Martone, P. Rizzoli, U. Steinbrecher, J.W. Antony, F.D. Zan, I. Hajnsek, K. Papathanassiou, F. Kugler, M.R. Cassola, M. Younis, S. Baumgartner, P. López-Dekker, P. Prats, A. Moreira, Tandem-x: a radar interferometer with two formation-flying satellites, Acta Astronaut. 89 (2013) 83–98, https://doi.org/10.1016/j.actaastro.2013.03.008.

[5] R. Kahle, H. Runge, J.-S. Ardaens, S. Suchandt, R. Romeiser, Formation flying for along-track interferometer oceanography-first in-flight demonstration with tandem-x, Acta Astronaut. 99 (2014) 130–142, https://doi.org/10.1016/j.actaastro.2014.02.014.

[6] S. D'Amico, J.-S. Ardaens, S.D. Florio, Autonomous formation flying based on gps - prisma flight results, Acta Astronaut. 82 (2013) 69–79, https://doi.org/10.1016/j.actaastro.2012.04.033.

[7] S. Persson, S. Veldman, P. Bodin, Prisma - a formation flying project in implementation phase, Acta Astronaut. 65 (2009) 1360–1374, https://doi.org/10.1016/j.actaastro.2009.03.067.

[8] U. Ahsun, D. Miller, J. Ramirez, Control of electromagnetic satellite formations in near-Earth orbits, J. Guid. Control Dyn. 33 (1883–1891) (2010), https://doi.org/10.2514/1.47637.

[9] E. Kong, D. Kwon, S. Schweighart, L. Elias, Electromagnetic formation flight for multisatellite arrays, J. Spacecr. Rockets 41 (4) (2004) 659–666, https://doi.org/10.2514/1.2172.

[10] D.W. Kwon, Propellantless formation flight applications using electromagnetic satellite formations, Acta Astronaut. 67 (2010) 1189–1201, https://doi.org/10.1016/j.actaastro.2010.06.042.

[11] E. Fabacher, S. Lizy-Destrez, D. Alazard, F. Ankersen, A. Profizi, Guidance of magnetic space tug, Adv. Space Res. 60 (2017) 14–27, https://doi.org/10.1016/j.asr.2017.03.042.

[12] Y. Qin, X. Lang, Passivity-based fractionated payload 6-dof maneuver control using electromagnetic actuation, Aerosp. Sci. Technol. 147 (2024) 109056, https://doi.org/10.1016/j.ast.2024.109056.

[13] C. Wei, X. Wu, B. Xiao, J. Wu, C. Zhang, Adaptive leader-following performance guaranteed formation control for multiple spacecraft with collision avoidance and connectivity assurance, Aerosp. Sci. Technol. 120 (2022) 107266, https://doi.org/10.1016/j.ast.2021.107266.

[14] U. Tancredi, A. Renga, M. Grassi, Validation on flight data of a closed-loop approach for GPS-based relative navigation of LEO satellites, Acta Astronaut. 86 (2013) 126–135, https://doi.org/10.1016/j.actaastro.2013.01.005.

[15] F. Causa, A. Renga, M. Grassi, Robust filter setting in GPS-based relative positioning of small-satellite LEO formations, Adv. Space Res. 62 (2018) 3369–3382, https://doi.org/10.1016/j.asr.2018.03.020.

[16] M. D'Errico, Distributed Space Missions for Earth System Monitoring, Springer, 2012, pp. 599–638.

[17] K. Gunnam, D.C. Hughes, J.L. Junkins, N. Kehtarnavaz, A vision-based dsp embedded navigation sensor, IEEE Sens. J. 2 (5) (2002) 428–442, https://doi.org/10.1109/JSEN.2002.806212.

[18] K. Matsuka, A.O. Feldman, E.S. Lupu, S.-J. Chung, F.Y. Hadaegh, Decentralized formation pose estimation for spacecraft swarms, Adv. Space Res. 67 (2021) 3527–3545, https://doi.org/10.1016/j.asr.2020.06.016.

[19] G. Napolano, C. Vela, A. Nocerino, R. Opromolla, M. Grassi, A multi-sensor optical relative navigation system for small satellite servicing, Acta Astronaut. 207 (2023) 167–192, https://doi.org/10.1016/j.actaastro.2023.03.008.

[20] M.A. Nurge, R.C. Youngquist, S.O. Starr, A satellite formation flying approach providing both positioning and tracking, Acta Astronaut. 122 (2016) 1–9, https://doi.org/10.1016/j.actaastro.2016.01.010.

[21] F.H. Raab, E.B. Blood, T.O. Steiner, H.R. Jones, Magnetic position and orientation tracking system, IEEE Trans. Aerosp. Electron. Syst. AES-15 (5) (1979) 709–718.

[22] E. Prigg, J. How, Signal architecture for a distributed magnetic local positioning system, IEEE Sens. J. 4 (6) (2004) 864–873.

[23] D. Lin, X. Chen, Mathematical models of 3d magnetic field and 3d positioning system by magnetic field, Appl. Math. Inf. Sci. 8 (4) (2014) 1647–1654.

[24] R.C. Youngquist, M.A. Nurge, S.O. Starr, Alternating magnetic field forces for satellite formation flying, Acta Astronaut. 84 (2013) 197–205, https://doi.org/10.1016/j.actaastro.2012.11.012.

[25] Y. Takahashi, H. Sakamoto, S. Sakai, Kinematics control of electromagnetic formation flight using angular-momentum conservation constraint, J. Guid. Control Dyn. 45 (2) (2022), https://doi.org/10.2514/1.G005873.
[26] Z. Abbasi, J. Hoagg, T.M. Seigler, Decentralized position and attitude control for electromagnetic formation flight, in: AIAA Scitech 2019 Forum, No. AIAA 2019-0908, San Diego, California, 2019.
[27] W.H. Clohessy, R.S. Wiltshire, Terminal guidance system for satellite rendezvous, J. Aerosp. Sci. 27 (9) (1960) 653–658, https://doi.org/10.2514/8.8704.
[28] K. Yamanaka, F. Ankersen, New state transition matrix for relative motion on an arbitrary elliptical orbit, J. Guid. Control Dyn. 25 (1) (2002), https://doi.org/10.2514/2.4875.
[29] S.J. Julier, J.K. Uhlmann, H. Durrant-Whyte, A new approach for filtering nonlinear systems, in: Proceedings of 1995 American Control Conference - ACC'95 3 (June), 1995, pp. 1628–1632.